polymers

MDPI

Article

Influence of PDMS Molecular Weight on Isothermal Crystallization in PDMS and PDMS–Zeolite Composites: A DSC and ESR Spin Probe Study

Tatjana Antonić Jelić [1,*], Lidija Androš Dubraja [1], Dalibor Merunka [1], Miroslava Lukešová [1], Fraser John MacMillan [2], Marin Tota [3] and Srećko Valić [1,3,4,*]

[1] Rudjer Bošković Institute, Bijenička Cesta 54, 10000 Zagreb, Croatia; lidija.andros@irb.hr (L.A.D.); dalibor.merunka@irb.hr (D.M.); miroslava.lukesova@irb.hr (M.L.)
[2] Institute of Physics, Bijenička Cesta 46, 10000 Zagreb, Croatia; fmacmillan@ifs.hr
[3] Faculty of Medicine, University of Rijeka, Braće Branchetta 20, 51000 Rijeka, Croatia; marin.tota@uniri.hr
[4] Centre for Micro and Nano Sciences and Technologies, University of Rijeka, Radmile Matejčić 2, 51000 Rijeka, Croatia
* Correspondence: tantonic@irb.hr (T.A.J.); valic@irb.hr or svalic@uniri.hr (S.V.)

Abstract

This study investigates the influence of polydimethylsiloxane (PDMS) molecular weight on crystallization kinetics and molecular dynamics in pristine PDMS and PDMS–zeolite composites. Three PDMS samples with molecular weights of 4,000, 28,000, and 63,000 were examined. Zeolite A with spherical particle morphology was used as a filler, and composites containing 30 wt% zeolite were prepared. Crystallization kinetics and thermal behavior were investigated by differential scanning calorimetry (DSC), while changes in the local molecular dynamics of the amorphous phase during isothermal crystallization at −85 °C were monitored by electron spin resonance (ESR) using the spin probe method. Both DSC and ESR results demonstrate that the presence of zeolite accelerates isothermal crystallization, regardless of PDMS molecular weight, with the most pronounced effect observed for the intermediate molecular weight (28,000). Avrami analysis further confirms the strong influence of molecular weight on crystallization kinetics, with higher molecular weight PDMS crystallizing more rapidly in both pristine and zeolite-filled systems. The close correspondence between the characteristic times determined by DSC and ESR indicates a strong relationship between crystal formation and changes in the molecular dynamics of the remaining amorphous phase. Subsequent DSC heating scans revealed differences in melting behavior, with strongly overlapping melting endotherms for pristine low molecular weight PDMS and the corresponding zeolite composite, and clearly resolved double melting peaks for the higher molecular weight samples, suggesting differences in the stability and organization of the crystalline regions.

Keywords: polydimethylsiloxane (PDMS); PDMS–zeolite composites; isothermal crystallization; molecular weight; electron spin resonance (ESR); spin-probe method; differential scanning calorimetry (DSC)

Check for updates

Academic Editor: Małgorzata Maciejewska

Received: 13 October 2026
Revised: 31 October 2026
Accepted: 4 November 2026
Published: 10 November 2026

Copyright: © 2026 by the authors. Licensee MDPI, Basel, Switzerland. This article is an open access article distributed under the terms and conditions of the Creative Commons Attribution (CC BY) license.

1. Introduction

It is well known that polydimethylsiloxane (PDMS) chain segments can spatially organize and form crystalline structures under low-temperature conditions or upon application

of an external force [1–20]. These processes are known as temperature-induced crystallization and strain-induced crystallization, respectively. Among the parameters affecting PDMS crystallization, molecular weight is of particular interest because it influences chain mobility, local chain order, and crystallization kinetics [8,9]. Previous studies have further shown that the molecular dynamics of the amorphous phase, particularly local segmental mobility, are closely coupled to the development and stability of the crystalline phase [9–13]. However, the relationship between molecular weight, amorphous-phase dynamics, and isothermal crystallization kinetics has not been fully established. This question becomes particularly relevant in filled systems, where polymer–filler interfaces introduce additional constraints that may alter chain mobility and crystallization behavior [3,4,7,13,14,21,22].

In our previous study, we demonstrated that zeolite morphology and loading significantly affect the local segmental dynamics and crystallization behavior of PDMS–zeolite composites [13]. Zeolite incorporation was found to increase the isothermal crystallization rate and to modify the segmental mobility of PDMS in the amorphous phase, with the magnitude of the effect depending more strongly on zeolite morphology than on filler loading [13]. These findings indicate that the presence and structural characteristics of zeolite can modify the relationship between molecular mobility and crystallization in PDMS. However, the role of the molecular weight of the PDMS matrix in this process remains unclear. An important question is whether molecular weight affects crystallization kinetics only through changes in polymer-chain dynamics or also by modifying the influence of the polymer–zeolite interface on crystallization.

Previous ESR spin probe studies of semicrystalline PDMS by Massa and co-workers [11] have revealed the presence of two dynamically distinct amorphous fractions: the rigid amorphous fraction (RAF), associated with regions of restricted molecular mobility near crystalline domains, and the mobile amorphous fraction (MAF), characterized by higher molecular mobility. These studies also demonstrated the close relationship between the molecular dynamics of the amorphous phase and the crystalline organization of PDMS. Dielectric spectroscopy studies have independently shown that crystallization affects the molecular dynamics of the amorphous phase in PDMS [23,24]. In particular, Lund and co-workers [24] distinguished between the conventional amorphous phase (AP) and the constrained amorphous phase (CAP), which may correspond to MAF and RAF observed by ESR, respectively. Their results showed that the fraction of the constrained amorphous phase increases during crystallization, while the conventional amorphous phase gradually disappears.

Based on our previous results [13], zeolite A with spherical particle morphology was selected to investigate the influence of PDMS molecular weight on isothermal crystallization in pristine PDMS and PDMS–zeolite composites. To distinguish the effect of molecular weight from that of filler morphology and concentration, composites containing 30 wt% of spherical zeolite A were prepared with PDMS samples of different molecular weights. Crystallization kinetics and molecular dynamics were investigated by two complementary techniques: differential scanning calorimetry (DSC) and electron spin resonance (ESR) spectroscopy using the spin probe method. DSC was used to monitor isothermal crystallization kinetics and subsequent melting behavior, while ESR provided information on changes in the local molecular dynamics of the remaining amorphous phase during crystallization. By combining these techniques, the present study aims to clarify how PDMS molecular weight influences crystallization kinetics and the accompanying changes in amorphous phase dynamics, both in pristine PDMS and in the presence of zeolite.

2. Materials and Methods

2.1. Sample Preparation

Trimethylsiloxy-terminated polydimethylsiloxane (PDMS) samples with weight-average molecular weights (M_w) of 4,000, 28,000, and 63,000 were purchased from Thermo Fisher Scientific (Kandel, Germany). The free nitroxide radical 4-oxo-2,2,6,6-tetramethyl-1-piperidinyloxy (4-oxo-TEMPO or TEMPONE), used as a spin probe for ESR measurements, was purchased from Sigma-Aldrich (St. Louis, MO, USA). Zeolite A with spherical particle morphology was synthesized following the procedure described in the literature [25–28]. The particle size ranges from 0.4 µm to 5 µm, with 50% of the particles smaller than 1.45 µm and 90% smaller than 2.35 µm. The external specific surface area ranges from 2.37 m^2g^{-1} to 4.43 m^2g^{-1}, as previously reported [25]. The synthesized zeolite A was dried at 105 °C for 24 h to remove surface-adsorbed water, following the procedure described in reference [26]. After drying, the samples were stored in sealed plastic containers to minimize moisture readsorption prior to preparation of the PDMS–zeolite composites. The composition and labels of investigated samples are presented in Table 1.

Table 1. Chemical composition and labels of the investigated samples. Zeolite A with a spherical morphology was used as a filler.

Matrix	M_w	Filler / %	Label
PDMS	4,000	0	4K
		30	4KZ
	28,000	0	28K
		30	28KZ
	63,000	0	63K
		30	63KZ

PDMS–zeolite composites containing 30 wt% zeolite were prepared by directly mixing the filler with PDMS using a magnetic stirrer for 10 min at room temperature. The mixtures were subsequently placed in an ultrasonic bath and sonicated for 15 min to achieve a homogeneous dispersion of the filler particles within the PDMS matrix. All samples were prepared immediately prior to the measurements. A sedimentation test performed on the lowest molecular weight PDMS composite (4KZ) showed no visible particle sedimentation or macroscopic phase separation over 60 min at room temperature. The time between sample preparation and the onset of cooling to −85 °C for DSC and ESR measurements was considerably shorter than this period (less than 5 min).

For ESR measurements, the spin probe was incorporated into both pristine PDMS and PDMS–zeolite composites by directly mixing the nitroxide radical with the samples using a magnetic stirrer CUV-O-STIR, Model 332 (Hellma GmbH & Co. KG, Müllheim, Germany) for 10 min. The final spin-probe concentration was approximately 0.05 wt%.

2.2. DSC Measurements

Differential scanning calorimetry (DSC) thermograms were recorded on a Netzsch DSC 214 Polyma calorimeter (NETZSCH-Gerätebau GmbH, Selb, Germany). Approximately 10 mg of each sample was placed in aluminum pans for the measurements. Samples were cooled from room temperature to −85 °C at a rate of 40 °C/min. After reaching −85 °C, the heat flow was recorded isothermally as a function of time. The duration of the isothermal measurement was adjusted for each sample according to the time required for completion of the crystallization process. Following isothermal crystallization, the samples were heated to 20 °C at a rate of 10 °C/min to characterize the subsequent thermal transitions. All measurements were performed under a high purity nitrogen atmosphere at a flow rate

of 20 mL/min. The degree of crystallinity was calculated using the theoretical enthalpy value ΔHth = 37.4 Jg^{-1}, as reported in reference [4]. The measured enthalpy values of the composites were corrected for the zeolite content.

2.3. ESR Measurements

ESR measurements were performed on a Bruker EMX spectrometer (Bruker BioSpin GmbH, Rheinstetten, Germany), operating at 9.3 GHz, equipped with a Bruker ER 041 XG microwave bridge and a Bruker ER 4111 VT temperature control unit with an uncertainty of ±1 °C. The temperature of −85 °C, at which composite ESR spectra consisting of two components were observed, was chosen as the optimal temperature for characterizing the local motional behavior of PDMS chain segments. The samples were rapidly cooled (quenched) by direct insertion from room temperature into the ESR cavity maintained at −85 °C, without controlled cooling. All samples were then measured isothermally at this temperature as a function of time. The spectra were recorded every minute from the first minute until no change in spectral shape and line intensity was observed. The spectral parameters were: frequency 9.30 GHz, sweep width 100 G, sweep time 30.72 s, power 2.00 mW, modulation frequency 100 kHz, modulation amplitude 1.00 G, time constant 1.28 ms and receiver gain $1{\cdot}10^2$. WinEPR acquisition software, version 4.55, was used for spectrum acquisition and analysis.

All ESR spectra were simulated using the MATLAB R2026b-based toolbox EasySpin (version 6.0.15) [29]. For ESR data at −85 °C the "chilli" function for the slow motion regime was used to give accurate ESR parameters including the g-tensor elements (g), hyperfine coupling constants (a), rotational correlation times (τ_R), as well as the relative weightings for the two-component data. The parameters used for the ESR spectral simulations are summarized in Table S1 in the Supplementary Materials.

3. Results and Discussion

3.1. DSC Analysis

The DSC curves obtained from isothermal measurements of pristine PDMS and PDMS–zeolite composites with different molecular weights are presented in Figure 1. The heat flow was monitored as a function of time, with $t = 0$ defined as the moment when the sample reached the isothermal crystallization temperature of −85 °C. Figure 1 shows a pronounced molecular weight dependence of the isothermal crystallization behavior of pristine PDMS and the corresponding PDMS–zeolite composites, consistent with previous reports showing that PDMS crystallization kinetics strongly depend on molecular weight [8]. For the 63K samples, both pristine PDMS and the composite exhibit a relatively sharp exothermic peak within the first few minutes of the measurement, indicating rapid crystallization. The addition of zeolite therefore produces only a limited change in the overall crystallization time at this molecular weight. In contrast, the effect of zeolite is particularly pronounced for the 28K samples. Pristine PDMS (28K) exhibits a broad crystallization exotherm extending over a considerably longer time interval, whereas the corresponding composite displays a sharp exothermic peak shortly after reaching the isothermal temperature. This substantial shortening of the crystallization time suggests that the zeolite promotes heterogeneous nucleation [13] and substantially accelerates crystallization. Similar promotion of PDMS crystallization by inorganic silica surfaces has also been reported for PDMS–silica nanocomposites [22]. For the low molecular weight PDMS (4K) sample, the effect is considerably weaker. However, the composite 4KZ exhibits its peak maximum slightly earlier than pristine PDMS, while the completion of the crystallization process is also observed at an earlier stage, indicating that the presence of zeolite accelerates the crystallization process. The

influence of zeolite on PDMS crystallization is strongly dependent on molecular weight, with the most pronounced acceleration observed for the 28K sample.

The characteristic crystallization times derived from the isothermal DSC thermograms are summarized in Table 2. The parameter t_{max} denotes the time corresponding to the maximum of the crystallization exotherm, while t represents the time required for the crystallization process to be completed. The results reveal a strong dependence on molecular weight. The 4K sample exhibits the slowest crystallization, with t_{max} = 18 min and a total crystallization time of 35 min. The addition of zeolite slightly accelerates the process, reducing these values to 16 and 28 min, respectively. A much stronger effect is observed for the 28K sample, for which t_{max} decreases from 8.5 to 2 min and the crystallization time from 19 to 4 min upon incorporation of zeolite. For the 63K samples, crystallization is already rapid in pristine PDMS, t_{max} = 3 min and t = 4.5 min, while the corresponding composite shows only a modest further decrease to 2.5 and 3.5 min, respectively.

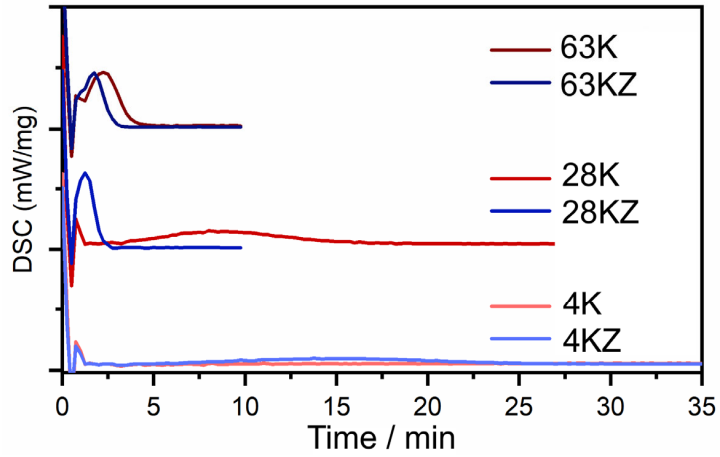

Figure 1. DSC curves of isothermal crystallization of pristine PDMS and PDMS-zeolite composites measured at −85 °C.

Table 2. Characteristic crystallization times obtained from isothermal DSC measurements of pristine PDMS and PDMS–zeolite composites. t_{max} denotes the time corresponding to the maximum of the crystallization exotherm, while t represents the time required for crystallization to be completed.

Sample	DSC	
	t_{max}/min	t/min
4K	18	35
4KZ	16	28
28K	8.5	19
28KZ	2	4
63K	3	4.5
63KZ	2.5	3.5

As discussed above, the presence of zeolite promotes heterogeneous nucleation, while the crystallization behavior of PDMS is strongly influenced by molecular weight. In the case of the 28KZ sample, the pronounced effect of zeolite therefore suggests that heterogeneous nucleation at the zeolite surface makes a particularly large contribution to the overall crystallization kinetics. Such behavior may be attributed to the interplay between nucleation, chain mobility, and chain transport during crystal formation. In the 63K sample, crystallization is already very rapid in the absence of zeolite, limiting the extent to which zeolite can further accelerate the process. In contrast, the shorter chains of the 4K sample may exhibit a different balance between molecular mobility and the ability to form stable crystalline domains, which could limit the effectiveness of additional nucleation sites. It should be

noted that differences in the degree of supercooling among PDMS samples of different molecular weights may also contribute to the observed differences in crystallization kinetics.

The isothermal crystallization kinetics at −85 °C were further analyzed using the Avrami equation [30,31]:

$$X(t) = 1 - \exp(-kt^n),$$

where $X(t)$ is the relative crystallinity at time t, k is the Avrami rate constant, and n is the Avrami exponent. The parameters n and k were determined from its linearized form:

$$\ln[-\ln(1 - X(t))] = \ln k + n \ln t.$$

The Avrami parameters, determined using relative crystallinity values in the range of 5% to 95%, reveal pronounced differences in crystallization behavior depending on both the molecular weight of PDMS and the presence of zeolite, Table 3. The corresponding Avrami plots, showing good linearity with high R^2 values, are provided in the Supplementary Materials Figure S1. For the 4K sample, the Avrami parameters could not be reliably determined due to the weak and broad crystallization exotherm. For pristine PDMS, the crystallization half-time, $t_{1/2}$, decreases markedly with increasing molecular weight, from 553 s for 28K to 133 s for 63K. This trend is consistent with the DSC results discussed above, which also indicate considerably slower crystallization of the low molecular weight 4K sample under the selected isothermal conditions, in agreement with previous studies reporting faster crystallization of higher molecular weight PDMS [8].

Table 3. Avrami parameters (n and k) and crystallization half-time ($t_{1/2}$) for isothermal crystallization at −85 °C. Avrami parameters for the 4K sample were not determined due to the weak and broad crystallization exotherm, which prevented reliable quantitative analysis.

Sample	n	k/s^{-n}	$t_{1/2}/s$
4K	-	-	-
4KZ	3.47	$4.12 \cdot 10^{-11}$	885
28K	3.91	$1.31 \cdot 10^{-11}$	553
28KZ	3.59	$1.09 \cdot 10^{-7}$	79
63K	3.44	$3.45 \cdot 10^{-8}$	133
63KZ	3.42	$1.00 \cdot 10^{-7}$	100

The incorporation of zeolite substantially accelerates crystallization, although the magnitude of this effect strongly depends on the molecular weight of PDMS. A pronounced effect is observed for 28K, for which $t_{1/2}$ decreases from 553 s to 79 s, i.e., by approximately a factor of seven. In contrast, the effect of zeolite is much less pronounced for 63K, where $t_{1/2}$ decreases only from 133 s to 100 s. Although a quantitative comparison based on Avrami parameters is not possible for 4K, the isothermal DSC curves also indicate an acceleration of crystallization upon zeolite addition. These findings are consistent with the DSC results and confirm that the major effect of zeolite is related to crystallization kinetics rather than to a simple increase in the final degree of crystallinity, as discussed below.

The Avrami exponent, n, ranges from 3.42 to 3.91 for the samples for which reliable parameters could be determined. The addition of zeolite results in relatively small changes in n for the 28K and 63K systems. Avrami-type crystallization kinetics have also been reported for PDMS, with an exponent of approximately 3 [24]. Since the Avrami exponent in polymer crystallization reflects a combination of nucleation behavior and crystal growth geometry, these values should not be interpreted as indicating a single idealized crystallization mechanism [30]. It should be noted that the Avrami parameters obtained in this study describe the crystallization kinetics during the isothermal stage rather than the overall crystallization process from the melt. Crystallization occurring during cooling may also influence these

parameters, particularly for the rapidly crystallizing 63K and 63KZ samples. Within these limitations, the relatively similar n values suggest that zeolite does not fundamentally alter the overall crystallization mechanism, but rather modifies the rate at which crystallization proceeds. This interpretation is consistent with the values of the Avrami rate constant, k, which increase upon zeolite addition for both the 28K and 63K systems.

Taken together, the Avrami analysis supports the conclusion obtained from the isothermal DSC measurements that zeolite predominantly acts by accelerating PDMS crystallization, with the magnitude of this effect strongly depending on molecular weight. The effect is particularly pronounced for 28K, whereas it becomes much less pronounced for 63K, which already exhibits rapid crystallization in the absence of zeolite. This suggests that the nucleating effect of zeolite is most significant when spontaneous crystallization of the polymer matrix is kinetically hindered. The role of zeolite as a heterogeneous nucleation agent in PDMS crystallization has also been suggested previously [13]. Once crystallization is already sufficiently rapid, as in 63K PDMS, the additional contribution of zeolite becomes comparatively small. To further assess whether these kinetic differences are accompanied by changes in the stability and degree of structural perfection of the crystals formed during isothermal crystallization, the subsequent heating scans were analyzed, as discussed below.

The resulting thermograms recorded after isothermal crystallization, Figure 2, reveal a double melting behavior, with two endothermic peaks denoted as T_{m1} and T_{m2}. The lower temperature endotherm may be associated with the melting of less stable and/or less perfectly organized crystallites, whereas the higher temperature peak may be attributed to more stable crystalline domains. In our previous study [13], an exothermic peak between two melting endotherms was observed for the same PDMS (28K) during heating at 10 °C/min following cooling to −150 °C, and was attributed to recrystallization. The occurrence of this peak was also found to depend on the type and content of zeolite, being clearly observed in pristine PDMS and certain zeolite composites, while absent in others. In contrast, no distinct exothermic peak is observed in the present study following isothermal crystallization at −85 °C, suggesting that significant recrystallization during subsequent heating is less likely, although some contribution from crystal reorganization cannot be completely excluded. The double melting behavior is particularly well resolved for the 28K and 63K samples. For pristine 28K PDMS T_{m1} and T_{m2} are −45.1 °C and −34.7 °C, respectively, and shift slightly to −44.3 °C and −34.1 °C upon the addition of zeolite. A similar shift toward higher temperatures is observed for the 63K system, from −43.8 °C and −35.0 °C to −43.3 °C and −34.4 °C, respectively. These small upward shifts of both melting temperatures may indicate slight differences in the thermal stability and/or reorganization behavior of the crystalline phase in the presence of zeolite. However, the individual melting enthalpies change only slightly: ΔH_{m1} and ΔH_{m2} change from 17.76 Jg^{-1} and 15.65 Jg^{-1} to 18.84 Jg^{-1} and 15.29 Jg^{-1}, respectively, for the 28K system, and from 14.01 Jg^{-1} and 16.60 Jg^{-1} to 13.34 Jg^{-1} and 16.46 Jg^{-1} for the 63K system. For the 4K samples, the two melting processes strongly overlap, preventing a reliable separation of their individual enthalpic contributions. Interestingly, the relative contributions of the two melting endotherms depend on PDMS molecular weight. While the lower-temperature endotherm has a slightly larger enthalpic contribution in the 28K samples, the higher-temperature endotherm becomes more prominent in the 63K samples, suggesting differences in the distribution of crystalline regions with different thermal stabilities.

Table 4 lists the enthalpy values measured during isothermal crystallization, ΔH_c. These values are consistently lower than the total melting enthalpy ΔH_m, and the difference between the two, $\Delta H = \Delta H_m - \Delta H_c$, may be primarily associated with crystallization occurring during cooling of the samples before reaching −85 °C ($t = 0$). However, a possible contribution from crystal reorganization during subsequent heating cannot be excluded.

A slight increase in ΔH_c is observed with increasing molecular weight of pristine PDMS from 20.13 Jg^{-1} for the 4K sample to 22.25 Jg^{-1} and 22.78 Jg^{-1} for the 28K and 63K samples, respectively. A more pronounced increase in ΔH_c is evident upon the addition of zeolite across all molecular weights. This is particularly notable in the medium molecular weight sample, where the value rises from 22.25 Jg^{-1} for pristine PDMS (28K) to 30.09 Jg^{-1} for the composite sample (28KZ). Comparing the ΔH_c values of composites with different molecular weights, an increase is also observed with increasing molecular weight, except for the highest molecular weight sample, 63KZ. In contrast, ΔH decreases with increasing molecular weight for both pristine PDMS and the composites, although this effect is less pronounced in the latter. This trend may indicate that molecular weight also influences crystallization during cooling, with a potentially greater extent of crystallization occurring at lower molecular weights. The presence of zeolite particles may affect segmental reorganization during cooling, while promoting subsequent isothermal crystallization by acting as heterogeneous nucleation sites [13]. The lowest molecular weight PDMS (4K) is expected to be essentially unentangled, whereas chain entanglement becomes increasingly important for the 28K and 63K samples. These differences, together with the higher viscosity at larger molecular weights, may influence molecular mobility and contribute to the observed differences in crystallization behavior. Under these conditions, zeolite particles may further modify crystallization during cooling.

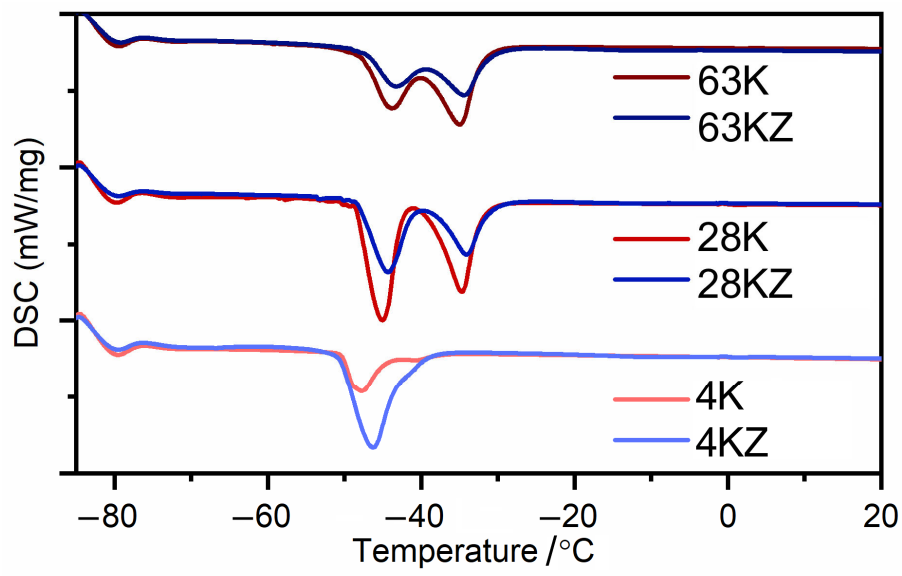

Figure 2. DSC curves obtained by heating the samples after isothermal crystallization at −85 °C.

Following isothermal crystallization at−85 °C, the total melting enthalpies of pristine PDMS and the corresponding zeolite composites are relatively similar, Table 4. The most striking example is the 28K system: although zeolite strongly accelerates crystallization, the total melting enthalpy increases only slightly, from 33.41 Jg^{-1} to 34.13 Jg^{-1}, corresponding to crystalline fractions of 89.33% and 91.25%, respectively. A similar trend is observed for the 4K and 63K samples. For 4K, the crystalline fraction changes only slightly from 88.24% to 86.44%, while for 63K it decreases from 81.85% to 79.68% upon addition of zeolite. The calculated degrees of crystallinity should be regarded as estimates based on the subsequent heating scans, since possible crystal reorganization and recrystallization during heating may influence their values. These results suggest that the main effect of zeolite is associated with crystallization kinetics rather than with a substantial increase in the apparent degree of crystallinity determined from the heating scans.

Table 4. Melting temperatures and enthalpies determined by DSC. ΔH_c is the enthalpy measured during isothermal crystallization; T_{m1} and T_{m2} represent the melting temperatures at lower and higher temperature ranges, respectively, while ΔH_{m1} and ΔH_{m2} correspond to the associated melting enthalpies. The total melting enthalpy, ΔH_m, is calculated as the sum of ΔH_{m1} and ΔH_{m2}, and ΔH is the difference between ΔH_m and ΔH_c. The values are reported for the investigated composites and pristine PDMS samples after isothermal crystallization at −85 °C. The enthalpy values of the composites are normalized to the PDMS mass.

Sample	ΔH_c /Jg^{-1}	T_{m1} /°C	T_{m2} /°C	ΔH_{m1} /Jg^{-1}	ΔH_{m2} /Jg^{-1}	ΔH_m /Jg^{-1}	ΔH /Jg^{-1}	χ_{m1} /%	χ_{m2} /%	χ /%
4K	20.13	−46.1	−40.5	33.00 [b]	[a]	33.00	12.87	88.24	-	88.24
4KZ	26.70	−46.3	−41.2	32.33 [b]	[a]	32.33	5.63	86.44	-	86.44
28K	22.25	−45.1	−34.7	17.76	15.65	33.41	11.16	47.49	41.84	89.33
28KZ	30.09	−44.3	−34.1	18.84	15.29	34.13	4.04	50.37	40.88	91.25
63K	22.78	−43.8	−35.0	14.01	16.60	30.61	7.83	37.46	44.39	81.85
63KZ	26.17	−43.3	−34.4	13.34	16.46	29.80	3.63	35.67	44.01	79.68

[a] Not determined separately due to strong overlap with the T_{m1} peak; its contribution is included in ΔH_{m1}. [b] Includes the enthalpic contributions of both overlapping melting endotherms.

3.2. ESR Analysis

The time evolution of the ESR spectra recorded during isothermal crystallization at −85 °C for pristine PDMS and the corresponding PDMS–zeolite composites is shown in Figure 3. The spectra exhibit pronounced changes in their line shapes with increasing crystallization time, reflecting changes in the molecular dynamics of the spin probe within the amorphous phase. Previous ESR studies of semicrystalline PDMS showed that spin probe molecules are excluded from the growing crystalline regions and remain distributed within the amorphous phase, where their motion reflects the local mobility and structural constraints imposed by the surrounding polymer chains [13]. Massa and coworkers [11] demonstrated the presence of dynamically distinct spin probe populations associated with the mobile amorphous fraction (MAF) and the rigid amorphous fraction (RAF). Consistent with these findings, our previous studies of PDMS–zeolite composites also demonstrated the presence of fast- and slow-motion ESR components associated with MAF and RAF, respectively [13]. As crystallization proceeds, the relative contributions of these components change, reflecting the progressive restriction of molecular mobility within the remaining amorphous phase.

To characterize the time evolution of the ESR spectra, two characteristic times were determined, Table 5. The time t_i represents the point at which the low field line intensities of the slow- and fast-motion components become equal, while t' corresponds to the time required to reach the steady state. Both characteristic times decrease with increasing PDMS molecular weight and upon the addition of zeolite. The most pronounced effect is observed for 28K, where t' decreases from 16 min for pristine PDMS to 4 min for the corresponding composite. For 4K and 63K, the addition of zeolite reduces t' from 40 min to 25 min and from 6 min to 3 min, respectively. In agreement with our previous observations of PDMS–zeolite composites, these results demonstrate that the presence of zeolite accelerates the evolution of molecular dynamics in the amorphous phase during isothermal crystallization [13].

A particularly interesting result is the close correspondence between the characteristic time t_i determined by ESR and the time t_{max} corresponding to the maximum crystallization rate obtained from DSC measurements, Figure 4. For all samples, these characteristic times are reasonably close, indicating that the redistribution between the MAF and RAF populations occurs on approximately the same timescale as the maximum rate of crystallization. This correspondence suggests a close relationship between crystal formation and the progressive restriction of molecular mobility in the remaining amorphous phase. Although the cooling procedures differ, with controlled cooling at 40 °C/min in DSC and rapid cooling

(quenching) in ESR, and differences in thermal history may influence crystallization kinetics, the observed agreement between the characteristic times remains noteworthy. Furthermore, the time required to reach the steady state in ESR measurements (t') is comparable to the time required for completion of crystallization determined by DSC. Thus, the two techniques provide complementary information on the kinetics of crystal formation and the accompanying changes in molecular dynamics.

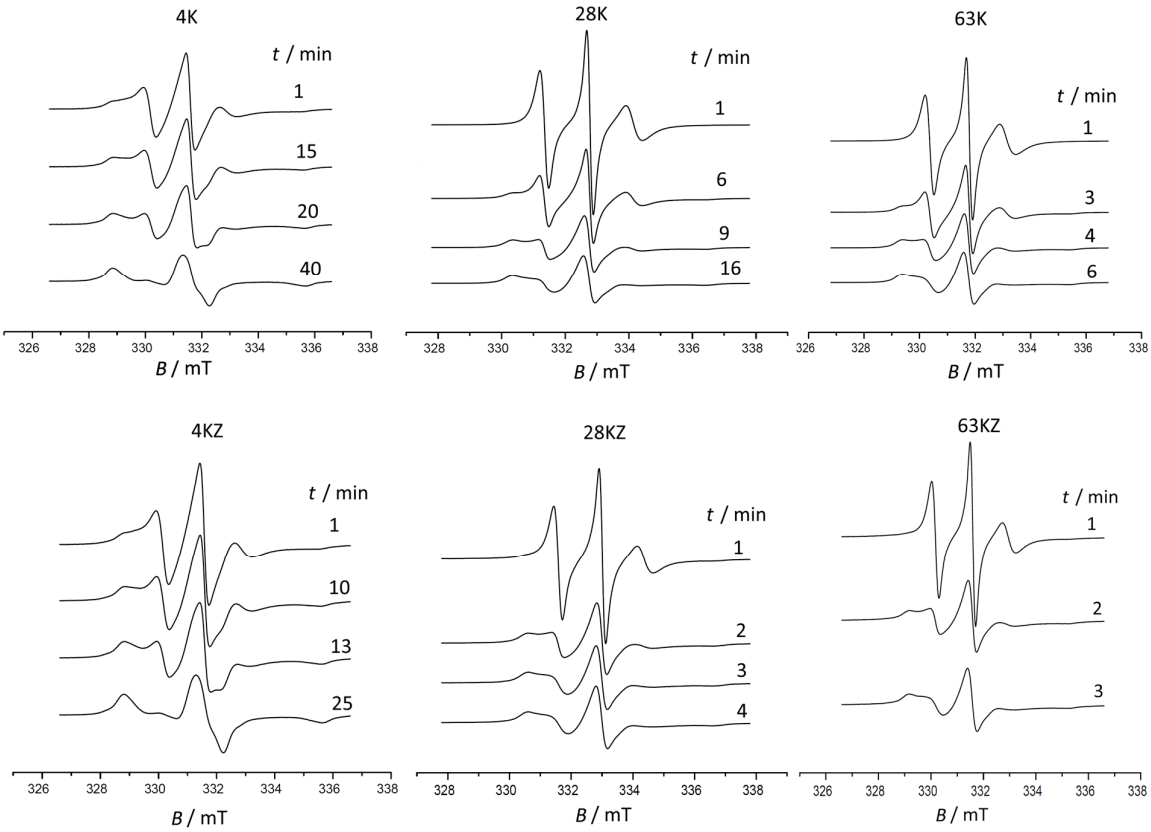

Figure 3. Time evolution of spin probe ESR spectra in pristine PDMS samples (4K, 28K, and 63K; upper panels) and the corresponding PDMS composites (4KZ, 28KZ, and 63KZ; lower panels).

Table 5. Characteristic times for spin probe motion in the amorphous phase during isothermal crystallization. t_i represents the time at which the low-field line intensities of the slow and fast components become equal, while t' is the time required to reach the steady state.

Sample	t_i/min	t'/min
4K	20	40
4KZ	13	25
28K	9	16
28KZ	2	4
63K	4	6
63KZ	2	3

To obtain more detailed information on the molecular dynamics of the amorphous phase, the ESR spectra were analyzed by two-component spectral simulations. An example of the experimental spectrum and its simulated slow- and fast-motion contributions is shown in Figure 5. A further example is provided in the Supplementary Materials Figure S2. The analysis provides the relative fractions of the slow (ϕ_s) and fast (ϕ_f) components, together with their corresponding rotational correlation times (τ_{Rs} and τ_{Rf}). The results obtained after 2 min at −85 °C and after reaching the steady state are summarized in Table 6.

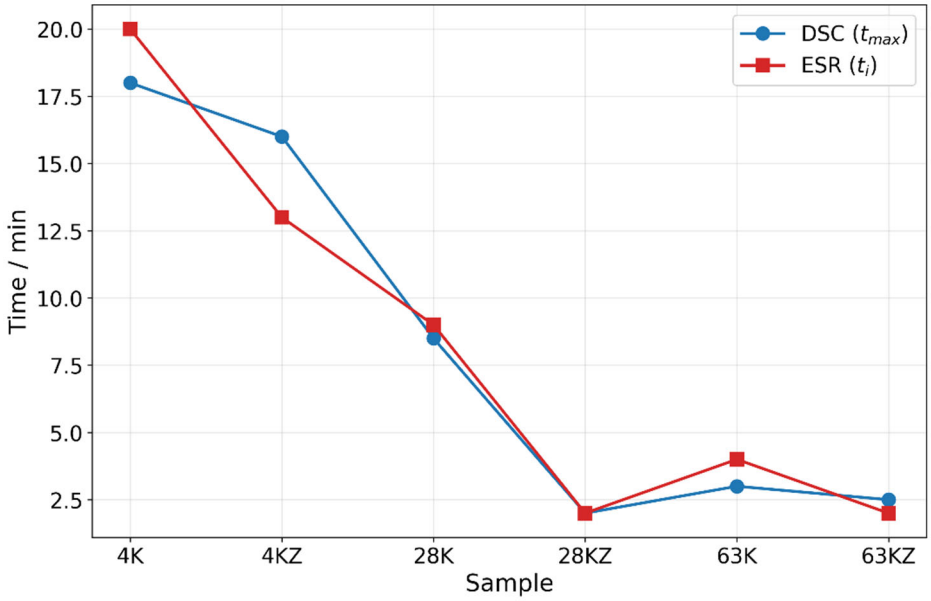

Figure 4. Comparison of the characteristic times obtained from DSC (t_{max}) and ESR (t_i) measurements during isothermal crystallization of pristine PDMS (4K, 28K, and 63K) and the corresponding PDMS–zeolite composites (4KZ, 28KZ, and 63KZ) at −85 °C.

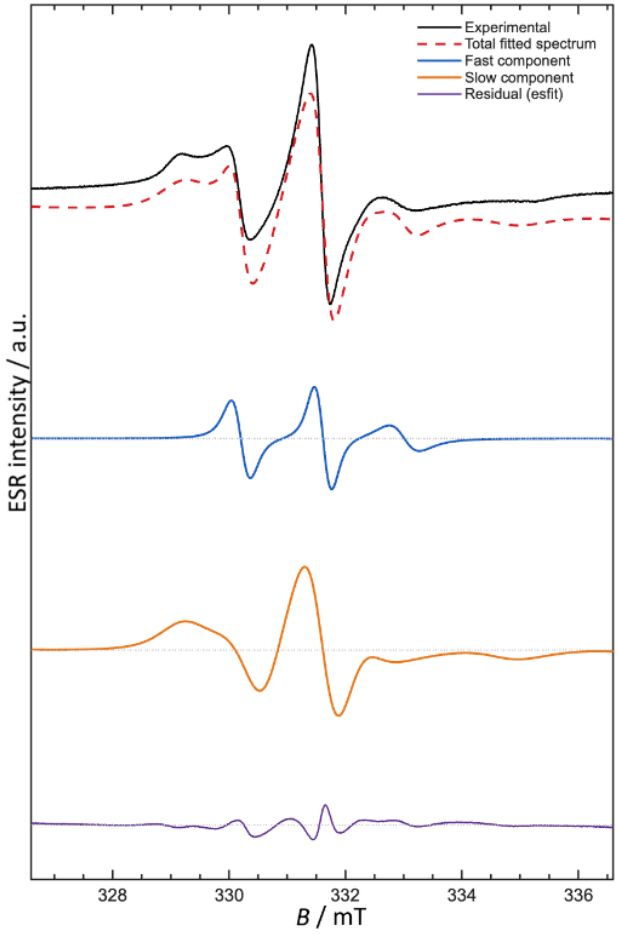

Figure 5. Experimental ESR spectrum (black line) of 63KZ after 2 min and the corresponding two-component simulation (red dotted line). The weighted contributions of the slow-(orange line) and fast-motion (blue line) components, as well as the residual (violet line), are shown separately. The simulated spectrum and individual components have been vertically offset for clarity.

Table 6. Analysis of the ESR spectra measured at −85 °C (a) after 2 min and (b) after the time t', required to reach the steady state. The fraction of the slow (ϕ_s) and fast (ϕ_f) components and their corresponding rotational correlation times (τ_{Rs} and τ_{Rf}, respectively) are shown.

(**a**)				
Sample	ϕ_s/%	ϕ_f/%	τ_{Rs}/ns	τ_{Rf}/ns
4K	15.6	84.4	133.9	4.9
4KZ	20.3	79.7	269.2	4.6
28K	18.2	81.8	8.9	3.2
28KZ	87.7	12.3	16.6	2.1
63K	30.1	69.9	18.0	2.5
63KZ	89.4	10.6	28.4	2.1
(**b**)				
Sample	ϕ_s/%	ϕ_f/%	τ_{Rs}/ns	τ_{Rf}/ns
4K	86.3	13.7	1250	5.3
4KZ	83.4	16.6	1450	3.4
28K	55.2	44.8	94.0	5.2
28KZ	87.3	12.7	17.9	3.9
63K	49.3	50.7	52.9	4.9
63KZ	75.0	25.0	37.4	3.0

After 2 min at −85 °C, the fraction of the slow component in pristine PDMS increases with molecular weight, from 15.6% for 4K to 18.2% for 28K and 30.1% for 63K, Figure 6. The addition of zeolite leads to a substantial increase in the slow component fraction for 28K and 63K, reaching 87.7% and 89.4%, respectively, whereas a much smaller increase is observed for 4K (from 15.6% to 20.3%). This pronounced molecular weight dependence is consistent with the faster crystallization of higher molecular weight PDMS and suggests that the development of crystalline regions is accompanied by the formation of amorphous environments with strongly restricted molecular mobility. However, since the extent of crystallization after 2 min differs considerably among the samples, these results primarily reflect differences in the progress of crystallization at a fixed time rather than only differences in the intrinsic mobility of the polymer chains.

At the steady state, the slow component fraction reaches 86.3% and 83.4% for 4K and 4KZ, respectively, while substantially lower values are observed for pristine 28K (55.2%) and 63K (49.3%). In contrast, the corresponding zeolite composites exhibit higher slow component fractions of 87.3% and 75.0%, respectively. These results indicate that the final distribution of dynamically distinct amorphous environments depends on both PDMS molecular weight and the presence of zeolite. The differences in the slow component fractions should not, however, be interpreted directly as differences in the total degree of crystallinity, since ESR and DSC probe different aspects of the semicrystalline structure.

Possible interactions between the spin probe molecules and the zeolite surface may also contribute to the slow ESR component. However, the presence of this component in pristine PDMS and its pronounced dependence on molecular weight suggest that its dominant contribution arises from restricted molecular mobility in the remaining amorphous phase rather than from direct spin probe–zeolite interactions, although the latter cannot be entirely excluded.

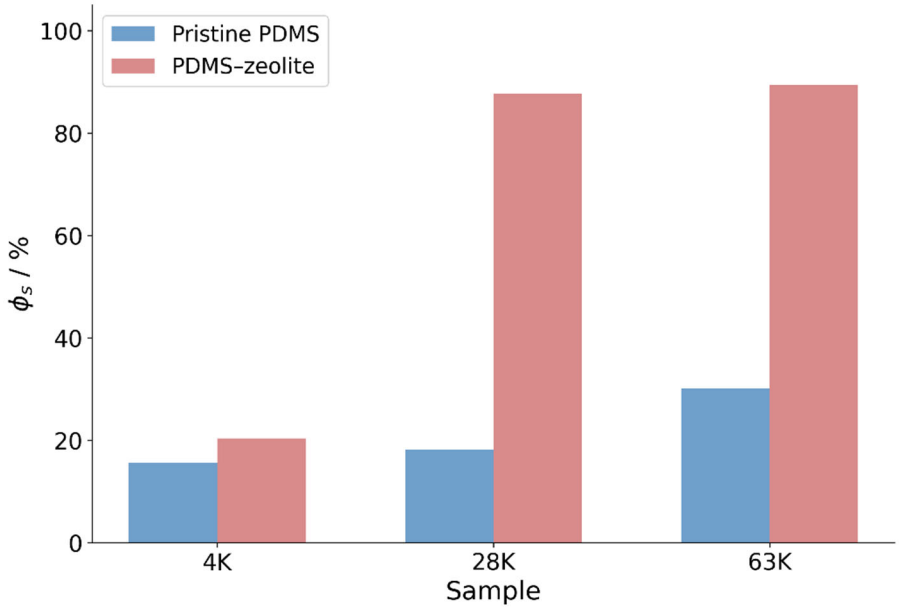

Figure 6. Fraction of the slow-motion ESR component (ϕ_s) in pristine PDMS (4K, 28K, and 63K) and the corresponding PDMS–zeolite composites (4KZ, 28KZ, and 63KZ), determined 2 min after reaching the isothermal crystallization temperature of −85 °C.

Further insight into the molecular dynamics of the amorphous phase is provided by the rotational correlation times, Table 6. Particularly high values of τ_{Rs} are obtained for 4K and 4KZ at the steady state (1250 ns and 1450 ns, respectively), indicating strongly restricted rotational motion of the spin probe in the slow motion component. However, such long correlation times approach the rigid-limit regime of X-band ESR, where their quantitative determination becomes less reliable. Therefore, they should primarily be regarded as indicators of strongly restricted molecular mobility rather than precise quantitative measures of rotational dynamics. Nevertheless, the pronounced difference compared with the higher molecular weight samples and their composites is also reflected in the ESR spectral line shapes at the steady state (Figure 3), which differ markedly between the 4K and 4KZ samples and those with higher molecular weights. Interestingly, although 4KZ and 28KZ exhibit similar fractions of the slow motion component, their rotational correlation times differ considerably. This indicates that similar fractions of the slow motion component do not necessarily imply similar molecular dynamics within the corresponding amorphous environments. The particularly slow probe motion observed for 4K and 4KZ may be related to their slower crystallization kinetics, which could allow more gradual reorganization of polymer chains and the development of amorphous environments with stronger restrictions on molecular mobility. The subsequent DSC heating scans show strongly overlapping melting endotherms for these samples, Figure 2, in contrast to the clearly resolved double melting behavior observed for 28K and 63K. Although this does not directly establish a higher degree of crystalline order, it suggests differences in the organization of crystalline regions that may also influence the molecular dynamics of the surrounding amorphous phase. This interpretation is consistent with the general concept of a rigid amorphous fraction in semicrystalline polymers, whose mobility is restricted by surrounding crystalline regions [32,33].

The ESR results indicate that the influence of zeolite extends beyond the acceleration of crystallization kinetics and also affects the distribution and molecular dynamics of the remaining amorphous phase. Combined with the DSC results, these findings demonstrate that PDMS molecular weight plays an important role in determining both the kinetics of

crystal formation and the local molecular dynamics of the remaining amorphous phase in pristine PDMS and PDMS–zeolite composites.

4. Conclusions

The isothermal crystallization behavior of pristine PDMS and PDMS–zeolite composites with different PDMS molecular weights was investigated at −85 °C using DSC and the ESR spin probe method. The results demonstrate a pronounced dependence of crystallization kinetics on PDMS molecular weight and the presence of zeolite. For both pristine PDMS and the corresponding composites, crystallization becomes faster with increasing molecular weight, while the addition of zeolite accelerates the process at all molecular weights investigated. The most pronounced effect of zeolite was observed for the intermediate molecular weight (28K), suggesting that the effect of zeolite addition on crystallization kinetics depends on PDMS molecular weight, possibly reflecting differences in polymer–zeolite interfacial interactions.

The Avrami analysis further confirmed the influence of molecular weight and zeolite on crystallization kinetics. DSC heating scans performed after isothermal crystallization suggested that zeolite primarily affects the crystallization rate rather than substantially increasing the final crystalline fraction.

The ESR results revealed pronounced changes in the molecular dynamics of the remaining amorphous phase during crystallization. The close correspondence between the characteristic times determined by ESR and DSC indicates a strong relationship between crystal formation and the redistribution of dynamically distinct amorphous populations. Furthermore, the differences in the fractions of the slow- and fast-motion components and their rotational correlation times demonstrate that the molecular dynamics of the remaining amorphous phase depend on both PDMS molecular weight and the presence of zeolite. Particularly high rotational correlation times observed for 4K and 4KZ at the steady state reveal strongly restricted local molecular mobility, suggesting a possible relationship between slower crystallization kinetics and the development of more constrained amorphous environments.

The combined DSC and ESR results provide complementary insight into the relationship between crystallization kinetics and molecular dynamics in PDMS and PDMS–zeolite composites, highlighting the important role of molecular weight and polymer–zeolite interactions in determining their crystallization behavior.

Supplementary Materials: The following supporting information can be downloaded at: https://www.mdpi.com/article/10.3390/polym18222806/s1, Figure S1: Avrami plots for the isothermal crystallization of pristine PDMS and PDMS–zeolite composites at −85 °C; Figure S2: Experimental ESR spectrum (black line) of 63K at the steady state and the corresponding two-component simulation (red dotted line); Table S1: Spin hamiltonian parameters, including g-tensor components and hyperfine coupling constants (A, in MHz), used in the ESR spectral simulations of pristine PDMS and PDMS–zeolite composites at −85 °C.

Author Contributions: Conceptualization, T.A.J. and S.V.; methodology, T.A.J. and S.V.; software, D.M. and F.J.M.; validation, T.A.J., L.A.D., M.L., S.V. and F.J.M.; formal analysis, T.A.J., L.A.D., S.V., M.L., F.J.M. and D.M.; investigation, T.A.J., L.A.D., M.L. and S.V.; resources, T.A.J., D.M. and S.V.; data curation, T.A.J., L.A.D., M.L., M.T. and S.V.; writing—original draft preparation, T.A.J. and S.V.; writing—review and editing, T.A.J. and S.V.; visualization, T.A.J., L.A.D., S.V., M.L., F.J.M. and M.T.; supervision, T.A.J. and S.V.; project administration, T.A.J. and S.V.; funding acquisition, S.V. and D.M. All authors have read and agreed to the published version of the manuscript.

Funding: This work was funded by the Croatian Science Foundation (project IP-2022-10-9292) and the University of Rijeka (project uniri-iz-25-235).

Data Availability Statement: The original contributions presented in this study are included in the article/Supplementary Material. Further inquiries can be directed to the corresponding authors.

Acknowledgments: During the preparation of this manuscript, the authors used ChatGPT Plus (version GPT-5.6 Sol) for the purposes of the literature review and generating Figures 4 and 6 and Graphical Abstract. The authors have reviewed and edited the output and take full responsibility for the content of this publication.

Conflicts of Interest: The authors declare no conflict of interest.

References

1. Damaschun, G. Röntgenographische Untersuchung der Struktur von Silikongummi, Kolloid-Z.u.Z. *Polymere* **1962**, *180*, 65–67. [CrossRef]
2. Clarson, S.J.; Dodgson, K.; Semlyen, J.A. Studies of cyclic and linear poly(dimethylsiloxanes): 19. Glass transition temperatures and crystallization behaviour. *Polymer* **1985**, *26*, 930–934. [CrossRef]
3. Ebengou, R.H.; Cohen-Addad, J.P. Silica-poly(dimethylsiloxane) mixtures: N.m.r. approach to the crystallization of adsorbed chains. *Polymer* **1994**, *35*, 2962–2969. [CrossRef]
4. Aranguren, M.I. Crystallization of polydimethylsiloxane: Effect of silica filler and curing. *Polymer* **1998**, *39*, 4897–4903. [CrossRef]
5. Albouy, P.-A. The conformation of poly(dimethylsiloxane) in the crystalline state. *Polymer* **2000**, *41*, 3083–3086. [CrossRef]
6. Dollase, T.; Spiess, H.W.; Gottlieb, M.; Yerushalmi-Rozen, R. Crystallization of PDMS: The effect of physical and chemical crosslinks. *Europhys. Lett.* **2002**, *60*, 390–396. [CrossRef]
7. Dollase, T.; Wilhelm, M.; Spiess, H.W.; Yagen, Y.; Yerushalmi-Rozen, R.; Gottlieb, M. Effect of Interfaces on the Crystallization Behavior of PDMS. *Interface Sci.* **2003**, *11*, 199–209. [CrossRef]
8. Maus, A.; Saalwächter, K. Crystallization Kinetics of Poly(dimethylsiloxane) Molecular-Weight Blends—Correlation with Local Chain Order in the Melt? *Macromol. Chem. Phys.* **2007**, *208*, 2066–2075. [CrossRef]
9. Klonos, P.A. Crystallization, glass transition, and molecular dynamics in PDMS of low molecular weights: A calorimetric and dielectric study. *Polymer* **2018**, *159*, 169–180. [CrossRef]
10. Massa, C.A.; Pizzanelli, S.; Bercu, V.; Pardi, L.; Bertoldo, M.; Leporini, D. A High-Field EPR Study of the Accelerated Dynamics of the Amorphous Fraction of Semicrystalline Poly(dimethylsiloxane) at the Melting Point. *Appl. Magn. Reson* **2014**, *45*, 693–706. [CrossRef]
11. Massa, C.A.; Pizzanelli, S.; Bercu, V.; Pardi, L.; Leporini, D. Constrained and Heterogeneous Dynamics in the Mobile and the Rigid Amorphous Fractions of Poly(dimethylsiloxane): A Multifrequency High-Field Electron Paramagnetic Resonance Study. *Macromolecules* **2014**, *47*, 6748–6756. [CrossRef]
12. Massa, C.A.; Pizzanelli, S.; Bercu, V.; Pardi, L.; Leporini, D. Local Reversible Melting in Semicrystalline Poly(dimethylsiloxane): A High-Field Electron Paramagnetic Resonance Study. *Macromolecules* **2017**, *50*, 5061–5073. [CrossRef]
13. Antonić Jelić, T.; Klepac, D.; Vratović, L.; Merunka, D.; Jurec, J.; Tota, M.; Galić, K.; Valić, S. The Effect of Zeolite Morphology and Loading on the Local Segmental Dynamics and Crystallisation Behaviour of PDMS-Zeolite Composites. *Polymers* **2025**, *17*, 2911. [CrossRef] [PubMed]
14. Fragiadakis, D.; Pissis, P.; Bokobza, L. Glass transition and molecular dynamics in poly(dimethylsiloxane)/silica nanocomposites. *Polymer* **2005**, *46*, 6001–6008. [CrossRef]
15. Albouy, P.-A.; Vieyres, A.; Pérez-Aparicio, R.; Sanséau, O.; Sotta, P. The impact of strain-induced crystallization on strain during mechanical cycling of cross-linked natural rubber. *Polymer* **2014**, *55*, 4022–4031. [CrossRef]
16. Shi, X.; Albouy, P.-A.; Launois, P. Strain-induced changes of the X-ray diffraction patterns of cross-linked Poly(dimethylsiloxane): The texture hypothesis. *Polymer* **2022**, *247*, 124760. [CrossRef]
17. Zhao, J.; Chen, P.; Lin, Y.; Chang, J.; Lu, A.; Chen, W.; Meng, L.; Wang, D.; Li, L. Stretch-Induced Crystallization and Phase Transitions of Poly(dimethylsiloxane) at Low Temperatures: An in Situ Synchrotron Radiation Wide-Angle X-ray Scattering Study. *Macromolecules* **2018**, *51*, 8424–8434. [CrossRef]
18. Zhao, J.; Feng, S.; Zhang, W.; Chen, W.; Sheng, J.; Yu, W.; Li, L. Strain Rate Dependence of Stretch-Induced Crystallization and Crystal Transition of Poly(dimethylsiloxane). *Macromolecules* **2021**, *54*, 9204–9216. [CrossRef]
19. Zhao, J.; Chen, P.; Lin, Y.; Chen, W.; Lu, A.; Meng, L.; Wang, D.; Li, L. Stretch-Induced Intermediate Structures and Crystallization of Poly(dimethylsiloxane): The Effect of Filler Content. *Macromolecules* **2020**, *53*, 719–730. [CrossRef]
20. Tosaka, M.; Noda, M.; Ito, K.; Senoo, K.; Aoyama, K.; Ohta, N. Strain- and temperature-induced polymorphism of poly(dimethylsiloxane). *Colloid Polym. Sci.* **2013**, *291*, 2719–2724. [CrossRef]
21. Yang, J.; Chen, Y.; Yang, Z.; Dai, L.; Choi, H.; Meng, Z. Unveiling the Nanoconfinement Effect on Crystallization of Semicrystalline Polymers Using Coarse-Grained Molecular Dynamics Simulations. *Polymers* **2024**, *16*, 1155. [CrossRef] [PubMed]

22. Bosq, N.; Guigo, N.; Persello, J.; Sbirrazzuoli, N. Melt and glass crystallization of PDMS and PDMS silica nanocomposites. *Phys. Chem. Chem. Phys.* **2014**, *16*, 7830–7840. [CrossRef] [PubMed]
23. Adachi, H.; Adachi, K.; Ishida, Y.; Kotaka, T. Dielectric relaxation of polydimethylsiloxane. *J. Polym. Sci. Polym. Phys. Ed.* **1979**, *17*, 851–857. [CrossRef]
24. Lund, R.; Alegría, A.; Goitandía, L.; Colmenero, J.; González, M.A.; Lindner, P. Dynamical and Structural Aspects of the Cold Crystallization of Poly(dimethylsiloxane) (PDMS). *Macromolecules* **2008**, *41*, 1364–1376. [CrossRef]
25. Subotic, B.; Kosanovic, C.; Bosnar, S.; Jelic, T.A.; Bronic, J. Zeolite 4a with New Morphological Properties, Its Synthesis and Use. WIPO (PCT) WO2010128342A1. 4 May 2010. Available online: https://patents.google.com/patent/WO2010128342A1/en (accessed on 15 July 2025).
26. Kosanović, C.; Jelić, T.A.; Bronić, J.; Kralj, D.; Subotić, B. Chemically controlled particulate properties of zeolites: Towards the face-less particles of zeolite A. Part 1. Influence of the batch molar ratio [SiO2/Al2O3]*b* on the size and shape of zeolite A crystals. *Microporous Mesoporous Mater.* **2011**, *137*, 72–82. [CrossRef]
27. Subotić, B.; Bronić, J.; Jelić, T.A. Chapter 6–Theoretical and Practical Aspects of Zeolite Nucleation. In *Ordered Porous Solids*; Valtchev, V., Mintova, S., Tsapatsis, M., Eds.; Elsevier: Amsterdam, The Netherlands, 2009; pp. 127–185. [CrossRef]
28. Antonić Jelić, T.; Bronić, J.; Hadžija, M.; Subotić, B.; Marić, I. Influence of the freeze-drying of hydrogel on the critical processes occurring during crystallization of zeolite A—A new evidence of the gel "memory" effect. *Microporous Mesoporous Mater.* **2007**, *105*, 65–74. [CrossRef]
29. Stoll, S.; Schweiger, A. EasySpin, a comprehensive software package for spectral simulation and analysis in EPR. *J. Magn. Reson.* **2006**, *178*, 42–55. [CrossRef] [PubMed]
30. Lorenzo, A.T.; Arnal, M.L.; Albuerne, J.; Müller, A.J. DSC isothermal polymer crystallization kinetics measurements and the use of the Avrami equation to fit the data: Guidelines to avoid common problems. *Polym. Test.* **2007**, *26*, 222–231. [CrossRef]
31. Toda, A. Crystallization kinetics, Avrami analysis, and fast-scanning DSC of polymers. *Polymer* **2025**, *332*, 128522. [CrossRef]
32. Wunderlich, B. Reversible crystallization and the rigid–amorphous phase in semicrystalline macromolecules. *Prog. Polym. Sci.* **2003**, *28*, 383–450. [CrossRef]
33. Schick, C.; Wurm, A.; Mohammed, A. Formation and disappearance of the rigid amorphous fraction in semicrystalline polymers revealed from frequency dependent heat capacity. *Thermochim. Acta* **2003**, *396*, 119–132. [CrossRef]

Disclaimer/Publisher's Note: The statements, opinions and data contained in all publications are solely those of the individual author(s) and contributor(s) and not of MDPI and/or the editor(s). MDPI and/or the editor(s) disclaim responsibility for any injury to people or property resulting from any ideas, methods, instructions or products referred to in the content.